

Final Technical Report

Award Number G13AP00042

**Study of Near-Source Geometrical Spreading and Radiation Pattern Effects from the
Aftershocks of the 2011 Virginia Earthquake**

Martin C. Chapman, John A. Hole, Jacob N. Beale, Qimin Wu and Sharmin Shamsalsadati

Department of Geosciences

Virginia Polytechnic Institute and State University

4044 Derring Hall, Blacksburg, Virginia, 24061

Phone (mcc): (540) 231-5036

Phone (jah): (540) 231-3858

Fax: (540) 231-3386

**Email: mcc@vt.edu (Chapman), hole@vt.edu (Hole), jbeale@vt.edu (Beale),
wqimin86@vt.edu (Wu), sharmin@vt.edu (Shamsalsadati),**

Project Period: July 2013 - December, 2014

Abstract

We used shallow aftershocks of the August 23, 2011 Mineral, Virginia, earthquake to study geometrical spreading at hypocentral distances less than 60 km. The data were obtained from a deployment of 30 three-component short period instruments along a northeast-trending profile extending approximately 60 km from the mainshock epicenter (AIDA array) and 29 additional off-profile stations surrounding the mainshock epicenter.

Sixteen of the largest aftershocks occurring in the time period from August 29, 2011 through November 3, 2011 provided the data. The analysis used the coda-normalization method to estimate the attenuation coefficient associated with geometrical spreading. The analysis examined the frequency dependence of attenuation of time-domain peak S-wave amplitudes by band-pass filtering the data in several octave-wide frequency bands, with center frequencies in the range from 2.0 to 22 Hz and constructing the envelope function. Amplitude-distance behavior was examined for the radial, transverse and vertical component peak S-wave, with corrections for SH and SV focal mechanism radiation pattern.

We observe no systematic frequency dependence. The geometrical spreading coefficients for the radial and transverse components, derived as a weighted mean over the entire range of frequencies (approximately 1.5 to 30 Hz), are -1.54 ± 0.02 and -1.71 ± 0.03 , respectively. The vertical component attenuation is less than the horizontals, with a weighted mean value of the attenuation coefficient over the entire range of frequencies of -1.37 ± 0.03 . The estimated attenuation coefficients differ significantly from the value of -1.0 expected for a homogenous whole space. The results for the horizontal components are in close agreement with previous modeling using full wavefield synthetics. However, the vertical component attenuation observed here is substantially less than that predicted by the synthetics. The focal depths of the shocks studied here are less than 8 km, with a mean depth of 5 km, and these results may not be representative of geometrical spreading in parts of eastern North America where shocks typically occur at greater depths.

Introduction

The data for studying ground motion propagation in the eastern United States are sparse in the near-source distance range most important for strong ground motion. Few seismic stations operate in most areas of the eastern U.S., and station spacing is several tens of kilometers or more over most of the region. As a result, data for the development of ground motion prediction models consists largely of recordings made at distances in excess of 120 km, beyond the range at which significant damage to structures usually occurs in the case of moderate earthquakes.

Because of the sparse data, most current ground motion prediction models for the eastern U.S. are based to some degree on the stochastic model (Hanks and McGuire, 1981; Boore, 1983; Atkinson and Boore, 1995; Toro et al., 1997; Boore 2003, Atkinson and Boore, 2006). The decay of ground motion amplitude with distance is modeled by quantifying two physical processes: 1) frequency independent attenuation (geometrical spreading) and 2) frequency-dependent attenuation, due to anelastic absorption and/or scattering. In the hypocentral distance range of

interest here (to approximately 60 km), geometrical spreading dominates, and is the more important of the two processes at frequencies of engineering concern.

Empirical studies, using data primarily from earthquakes in southeastern Canada and the northeastern United States, report relatively rapid decay of ground motion amplitude with hypocenter distance r , for r less than approximately 70 km. Less rapid decay is observed at distances exceeding approximately 120 km, and a zone of no attenuation (or increasing amplitude with distance) in the intervening distance range has been documented (Atkinson and Mereu, 1992, Atkinson, 2004). The flattening of apparent attenuation and/or increase in amplitude observed from approximately 70 to 120 km has been attributed to large amplitude post-critical reflections from the mid-lower crust and Moho (Burger et al., 1987, Atkinson, 2004). The Lg phase begins to develop at approximately 120 km or somewhat beyond, depending on crustal structure. Lg is a crust-guided phase involving the reflection and interference of multi-path shear waves interacting with the free surface and laterally extensive velocity contrasts in the crust and from the Moho. Lg travels with a group velocity of approximately 3.5 km/s and is the largest amplitude phase on all three components for a source in the crust at distances exceeding approximately 120 km. It can be treated as the superposition of higher-mode surface waves, exhibiting geometrical spreading as $r^{-0.5}$ (Wang and Herrmann, 1980; Herrmann and Kijko, 1983; Kennett, 1986). The geometrical spreading of Lg beyond approximately 120 km is well-represented in the existing data base. It has been observed that vertical and horizontal components of Lg are similar, with the H/V amplitude ratio being only slightly greater than 1 for rock sites (Atkinson, 2004; Atkinson, 1993; Siddiqi and Atkinson, 2002).

Geometrical spreading is well-constrained by observations at distances where Lg dominates the wavefield, but closer to the epicenter the direct S -wave arrival is the dominant phase and geometrical spreading is more complex. The amplitude behavior at distances less than 60 km is not well-constrained by observations. The data that are available show a large amount of scatter. Theoretically, much of this scatter of near-source amplitudes should be attributable to the effects of the S -wave radiation pattern.

This study examines attenuation at hypocentral distances less than 60 km. The data were collected by dozens of temporary seismic stations deployed to record the aftershocks of the August 23, 2011 Mineral, Virginia earthquake. The analysis makes use of 3-component recordings at high frequency collected from 16 aftershocks with m_{bLg} magnitudes ranging from 1.9 to 3.6. The focal depths of the earthquakes are less than 8 km, with average depth 5 km. The results of this study are representative of shallow shocks, which is not the situation in all parts of eastern North America, particularly in southeastern Canada and in the southern Appalachians to the west of the Blue Ridge, where earthquakes may occur at depths in excess of 20 km.

Data

Figure 1 shows the locations of seismic stations used in this study. The stations were deployed with two objectives. Thirty stations were deployed along a 60 km northeast-trending profile extending from near the mainshock epicenter to near Fredericksburg, Virginia to study

velocity structure and attenuation (Dreiling and Mooney, 2015; Davenport et al., 2015). These stations are referred to as the AIDA (Aftershock Imaging with Dense Arrays) profile, and involve 3-component 4-Hz geophones recorded at 100 samples per second (Figure 1, green circles). These instruments operated from September 1 through September 9, 2011. The off-profile stations shown as red triangles in Figure 1 were deployed to locate aftershocks and determine focal mechanisms, by different groups including the University of Memphis, Virginia Tech, Lehigh University, U.S. Geological Survey (USGS), and the Incorporated Research Institutions for Seismology (IRIS). Some of those stations operated for more than 1 year. The instruments were a mixture of short-period (2 Hz), and low and high-gain broadband instruments: data sampling was at 100 or 200 samples per second, depending on station.

The data used here were collected from 16 earthquakes (m_{bLg} 1.9 - 3.6) that occurred in the time period August 29 - November 3, 2011. Focal mechanisms for those shocks were determined using *P* and *S*-wave polarity and amplitude information, from the off-profile stations (Wu and Chapman, 2015). The focal mechanisms are shown in the inset map (Figure 1). Hypocenter locations, origin times and strike, dip and rake of both nodal planes are listed in Table 1. Figure 2 shows acceleration seismograms recorded by the AIDA profile stations from the September 5, 2011 event (m_{bLg} 3.1).

Table 1
Hypocenter Location and Focal Mechanism Solutions

Mo-Da	Hr:Mn:Sec*	Lat.°N	Lon.°W	Depth (km)	m_{bLg}	Strk ₁	Dip ₁	Rk ₁	Strk ₂	Dip ₂	Rk ₂
08-29	01:06:36.1	37.941	77.984	4.5	2.8	38	66	97	202	25	75
08-29	03:15:21.6	37.939	77.983	4.3	2.9	46	77	98	193	15	58
08-29	03:16:51.6	37.938	77.983	4.1	3.1	48	74	96	206	17	69
08-30	03:48:28.7	37.908	77.982	7.1	3.3	34	54	116	174	43	58
09-01	09:09:37.7	37.946	77.948	6.9	3.6	37	49	107	191	44	71
09-03	21:10:53.2	37.949	77.969	5.8	2.0	319	40	161	63	78	52
09-05	16:54:24.4	37.948	77.970	5.5	3.1	65	64	56	301	42	138
09-06	17:06:38.4	37.946	77.989	2.9	2.2	77	66	91	254	24	88
09-06	21:17:53.6	37.938	77.964	6.3	2.1	44	49	126	177	52	56
09-07	05:56:43.6	37.959	77.946	6.4	2.1	353	65	135	105	50	33
09-09	05:36:05.8	37.950	77.964	5.9	1.9	299	42	149	53	70	52
09-17	15:33:13.4	37.926	77.989	4.2	3.0	22	77	133	125	45	19
10-09	15:53:24.1	37.952	77.978	3.3	2.7	284	33	148	42	73	61
10-12	16:40:00.4	37.942	77.985	4.2	3.4	39	71	109	172	27	46
10-19	00:02:45.0	37.942	77.988	4.0	2.8	61	78	104	189	18	39
11-03	12:50:31.9	37.948	77.965	5.9	2.6	320	62	142	70	57	34

* Coordinated Universal Time

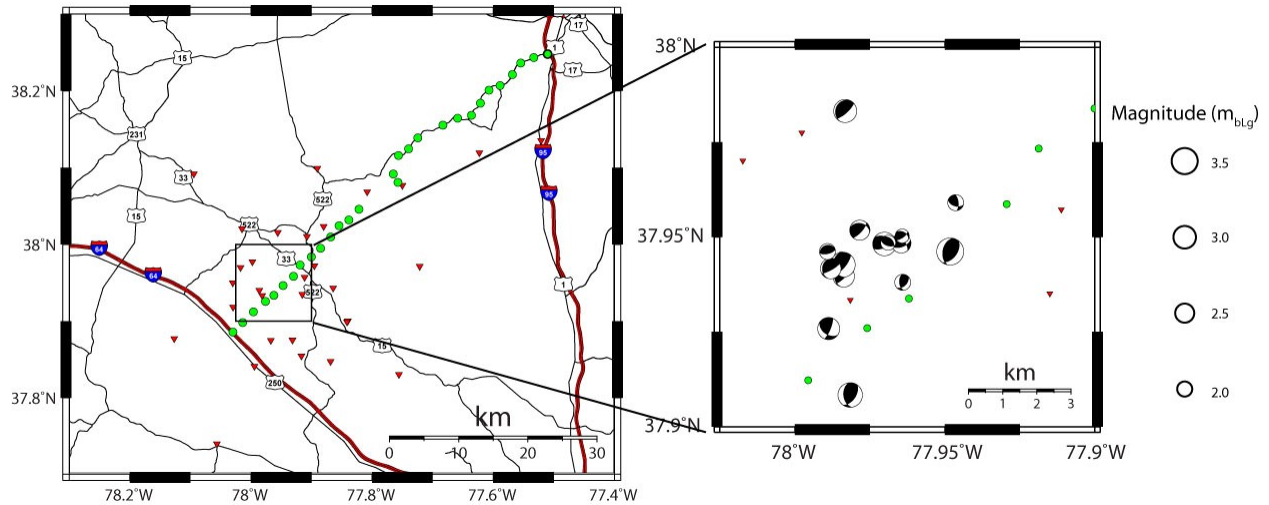


Figure 1. Map of study area showing the temporary station deployment for monitoring aftershock activity of the August 23, 2011 Mineral, Virginia earthquake. AIDA profile stations are shown as green circles and off-profile stations are shown by red triangles. Inset map shows locations and focal mechanism solutions of the 16 earthquakes used for analysis. Focal mechanisms are lower-hemisphere equal area projections, with P -wave compressional quadrants shaded, and with size scaled to m_{bLg} magnitude.

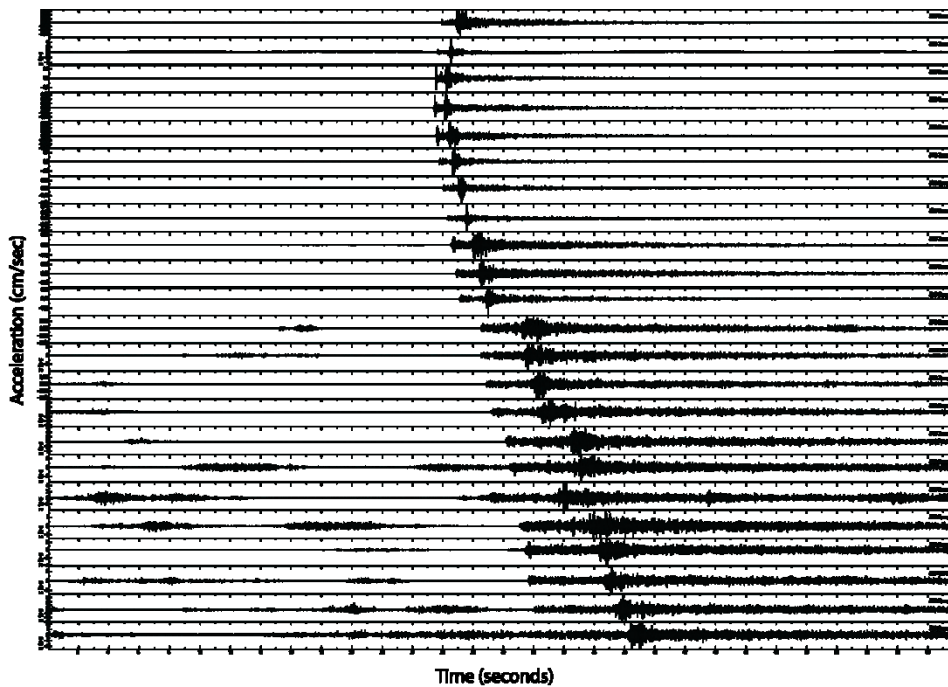


Figure 2: Vertical component (acceleration) recordings of the 16:54, Sept. 5, 2011 UTC aftershock recorded by the AIDA profiles stations.

Analysis

We use the coda-normalization method (Aki, 1980, Frankel et al., 1990) to quantify the attenuation of the S -wave. The method offers advantages for this study because the source spectrum, site response and instrument response are effectively cancelled by normalization of S -wave amplitudes using the coda wave amplitudes measured at a fixed lapse time.

The spectral amplitude $A(\omega, r)$ of the recorded shear wave as a function of frequency ω and hypocenter distance r can be represented by

$$A(\omega, r) = R S(\omega) B(\omega) I(\omega) r^{-\eta} e^{-\omega r / 2Q\beta}, \quad (1)$$

where R is the S -wave radiation pattern, $S(\omega)$ is the source spectrum, $B(\omega)$ is the site amplification, $I(\omega)$ is instrument response, η is the coefficient of geometrical spreading, Q is the S -wave quality factor and β is the S -wave velocity. The amplitude spectrum of the coda $A_c(\omega, t_l)$ at some lapse time t_l after the earthquake origin time can be represented as

$$A_c(\omega, t_l) = S(\omega) B(\omega) I(\omega) C(\omega, t_l), \quad (2)$$

where $C(\omega, t_l)$ is a function that describes the decay of coda as a function of frequency and lapse time (Frankel et al., 1990). Dividing Equation (1) by Equation (2) leads to

$$A(\omega, r) / A_c(\omega, t_l) = R r^{-\eta} e^{-\omega r / 2Q\beta} / C(\omega, t_l). \quad (3)$$

Normalizing the S -wave amplitude by dividing by the coda amplitude at a fixed lapse time removes the effects of the source spectrum, along with site and instrument response. Following Frankel et al. (1990), we assume that $C(\omega, t_l)$ is the same for all earthquakes and stations and is not dependent on focal depth. We assume that the coda, being made up of scattered S -waves that have taken a wide range of paths between source and receiver, is largely independent of source radiation pattern at a sufficiently large lapse time. Aki (1980) and many subsequent researchers have found that the coda amplitude decay is similar between multiple stations recording a given earthquake. This behavior is observed at lapse times in excess of approximately twice the S -wave travel time. Therefore, following coda-normalization according to Equation (3) for a fixed lapse time (say 2 times the S -wave travel time or greater), amplitude versus distance data from multiple earthquakes can be combined on a single plot (for a given frequency), allowing attenuation parameters to be estimated jointly. Assuming that n stations record m earthquakes, a system of $n \times m$ linear observational equations can be written for a given frequency ω :

$$Y_{ij} = \ln[A_{ij}(\omega, r_{ij}) / R_{ij}] - \ln[A_{c\ ij}(\omega, t_l)] = D - \eta \ln r_{ij} - \omega r_{ij} / 2Q\beta. \quad (4)$$

We follow Frankel et al. (1990) and Frankel (2015) and measure S -wave and coda amplitudes using the time-domain envelope function, derived from a series of narrow bandpass filtered seismograms. We use 9 octave-wide frequency bands, centered at frequencies 2.1, 2.81, 3.75, 5.06, 6.75, 9.0, 12.6, 16.88 and 22.5 Hz. The quantity $A_{ij}(\omega, r_{ij}) / R_{ij}$ in Equation (4) is here

taken to be the maximum envelope function amplitude in a 7 second time window following the predicted S-wave arrival time, at the i 'th station recording the j 'th earthquake, divided by the S-wave radiation pattern value for the j 'th earthquake and the i 'th station. The quantity $A_{c\ ij}(\omega, t_l)$ is the geometric mean value of the coda envelope function in a 5 second window beginning at lapse time $t_l = 28.9$ seconds following the origin time, corresponding to twice the direct S-wave travel time to a station at hypocentral distance 50 km (which is the maximum distance for this data set). We use data conditional on a signal/noise criterion such that the coda amplitude at lapse time 28.9 seconds exceeds that of the pre P-wave noise by a factor of 3. We consider three components of motion: radial, transverse and vertical, and treat the components separately. The SV radiation pattern term is used to correct the observed peak S-wave amplitudes on the vertical and radial components. The SH radiation pattern is used in connection with the transverse component.

The hypocentral distances involved in this study are less than 50 km. The recording sites are on weathered rock and residual soils, underlain at shallow depth by Paleozoic metamorphic rock with shear wave velocity in excess of 3.4 km/sec (Chapman, 2013, Dreiling and Mooney, 2015, Davenport et al., 2015). Assuming that frequency dependent anelastic absorption is negligible, Equation (4) can be written as

$$Y_{ij} = \ln[A_{ij}(\omega, r_{ij})/R_{ij}] - \ln[A_{c\ ij}(\omega, t_l)] = D - \gamma \ln r_{ij}, \quad (5)$$

where the constant D and the attenuation coefficient γ can be estimated by linear regression. The extent to which the assumption concerning high-frequency anelastic/scattering loss is viable can be assessed by examining any frequency dependent behavior of the regression estimates of γ , which in addition to geometrical spreading, here includes the effects of anelastic absorption/scattering of high frequencies at the more distant stations. If Q is sufficiently low, the estimates of γ from Equation (5) should increase with frequency.

Figure 3 shows, for example, the radial component coda-normalized envelopes for stations BUPP (7.5 km hypocenter distance) and PTRD (35.1 km hypocenter distance), from the m_{bLg} 3.6 earthquake at 09:09 UTC on Sept. 9, 2011, at several different frequencies. Figure 4 directly compares the coda-normalized envelopes for stations BUPP and PTRD for the 6.75 Hz center frequency.

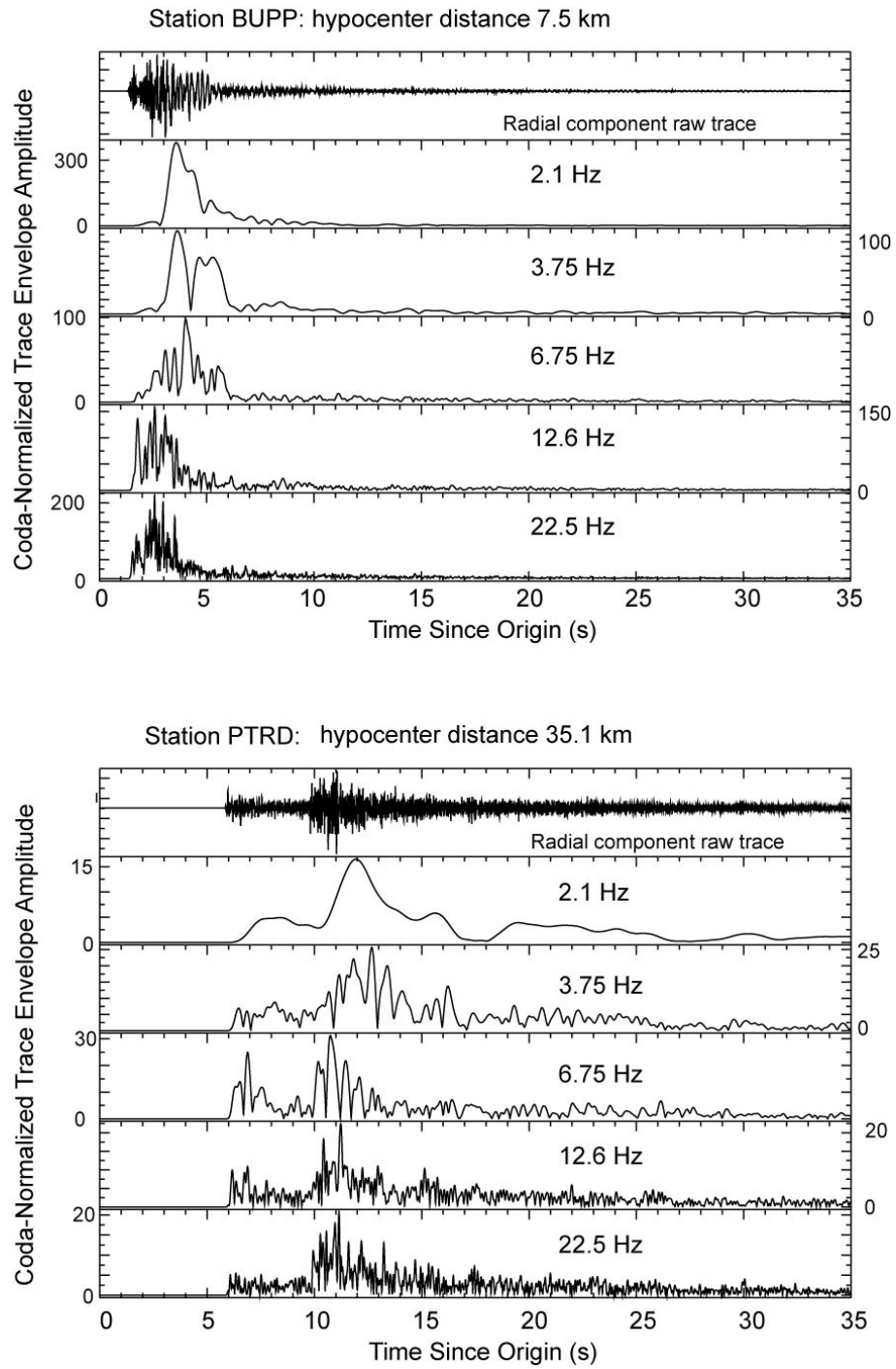


Figure 3: Radial component trace envelopes for stations BUPP (7.5 km hypocenter distance) and PTRD (35.1 km hypocenter distance), from the m_{bLG} 3.6 earthquake at 09:09 UTC on Sept. 9, 2011.

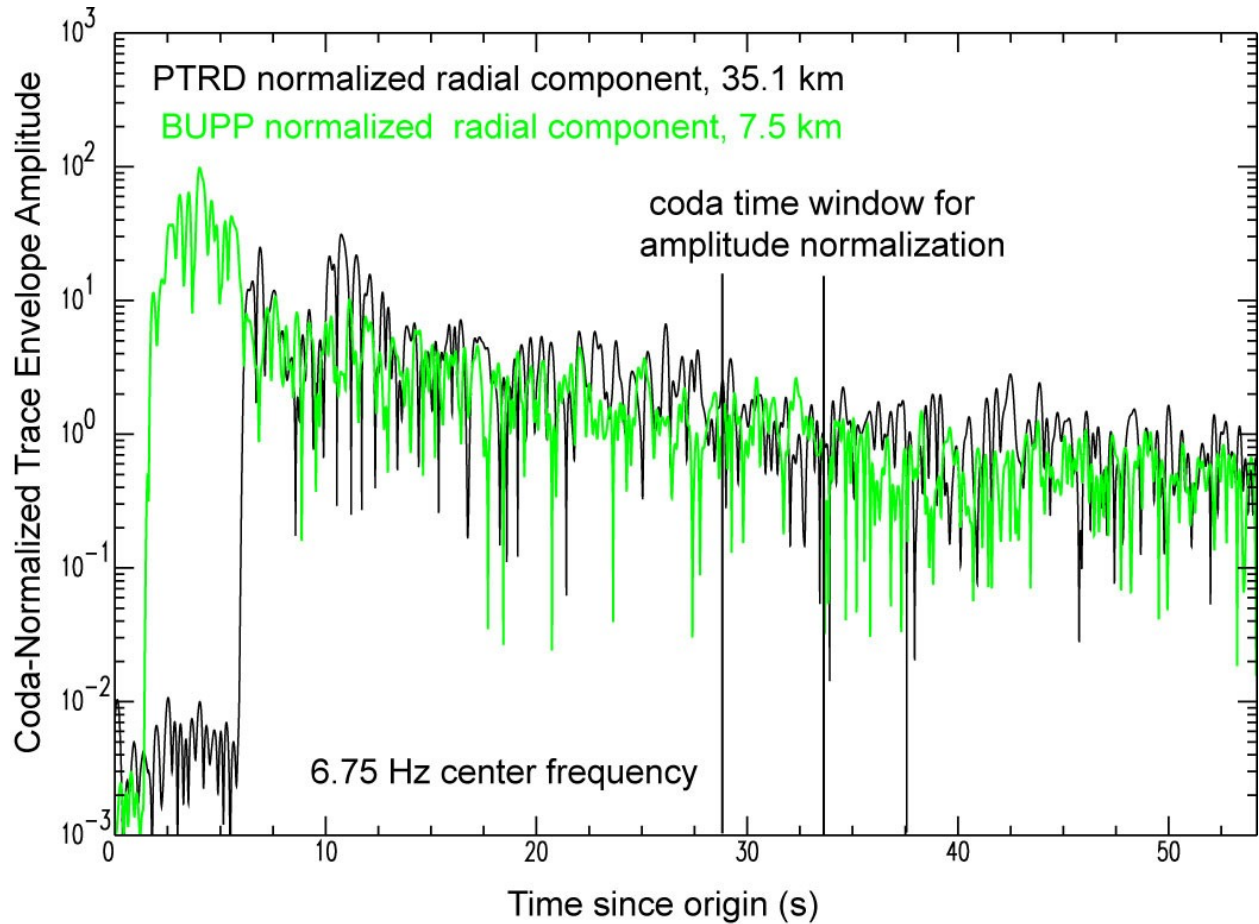


Figure 4. Radial component trace envelopes for stations BUPP (7.5 km hypocenter distance) and PTRD (35.1 km hypocenter distance), from the m_{bLg} 3.6 earthquake at 09:09 UTC on Sept. 9, 2011. The envelope functions are computed from traces filtered in an octave-wide frequency band centered at 6.75 Hz. The coda lapse time window used to establish the amplitude normalization is from 28.9 to 33.9 seconds after the earthquake origin time. Peak P and S -wave arrivals at PTRD are at approximately 6 and 12 seconds after origin time, respectively.

Results and Conclusions

Figure 5 shows the results of fitting regression models of the form of Equation (5) to the coda-normalized peak S-wave envelope amplitudes for the vertical, radial and transverse components in four of the nine frequency bands. The data exhibit geometrical spreading in excess of r^{-1} , which is indicated by the dashed lines in Figure 5. The estimates of $-\gamma$ in Equation (5) for the three components are shown, along with their +/- standard errors of estimate, in Figure 6.

There appears to be some systematic differences between the three components of motion. Surprisingly, the vertical component shows the least attenuation, with a weighted mean estimate over the 9 frequency bands of $\gamma = 1.37 \pm 0.03$. This differs substantially from the theoretical estimates for the vertical component derived by Chapman and Godbee (2012). Figure 7 shows that the theoretical modeling suggests γ of approximately 3.0 for the vertical component and a reverse fault at 7 km hypocenter depth. On the other hand, the results determined in this study for the radial and transverse components are 1.54 ± 0.02 and 1.71 ± 0.03 , respectively. Those values are close to those inferred from the theoretical modeling (γ approximately 1.6 for the shallow reverse fault). The transverse component here shows slightly more attenuation with distance than the radial component, but this is marginally significant, given the uncertainties. The values of γ do not show compelling evidence for systematic trends with frequency, implying small frequency-dependent effects from anelastic loss and scattering.

These results differ from those reported by Dreiling and Mooney (2015) from their study using Mineral earthquake aftershock data recorded by the AIDA profile stations. They examined peak time domain S-wave amplitudes in four octave-wide frequency passbands. For the geometric mean of the two horizontal components, they report $\gamma = 0.8$ (1-2 Hz), 0.9 (2-4 Hz), 1.05 (4-8 Hz) and 1.15 for 8-16 Hz. Dreiling and Mooney (2015) used a regression of peak S-wave envelope amplitude on hypocenter distance, but did not normalize the peak S-wave amplitudes using coda amplitudes as was done in this study. Also, this study used 29 off-profile stations in addition to the 30 AIDA profile stations, corrected for radiation pattern, and used a somewhat different set of earthquakes.

Frankel (2015) examined near-source S-wave attenuation in the Charlevoix, Quebec region using the coda-normalization method. Frankel used a set of 7 earthquakes with M_N magnitudes in the range 3.3-5.4, and focal depths from 6.5 to 24.5 km. Six of those events were at depths between 11 and 25 km, substantially deeper than those studied here (Table 1). Frankel (2015) observed attenuation similar to that found here at frequencies near 1 Hz, but found that attenuation decreases with increasing frequency, such that at frequencies near 14 Hz, γ is approximately 1.0. Frankel attributes this behavior to radiation pattern and directivity effects, resulting in larger apparent attenuation of the low frequencies. Insofar as the analysis methods are similar and the data here have been corrected for radiation pattern, the differences between this study and Frankel (2015) are puzzling. The divergent results (this study, Dreiling and Mooney, 2015, and Frankel, 2015) point to the general sensitivity of results to analysis methods, and possibly to the complicating role of un-modeled source effects, crustal structure and focal depth.

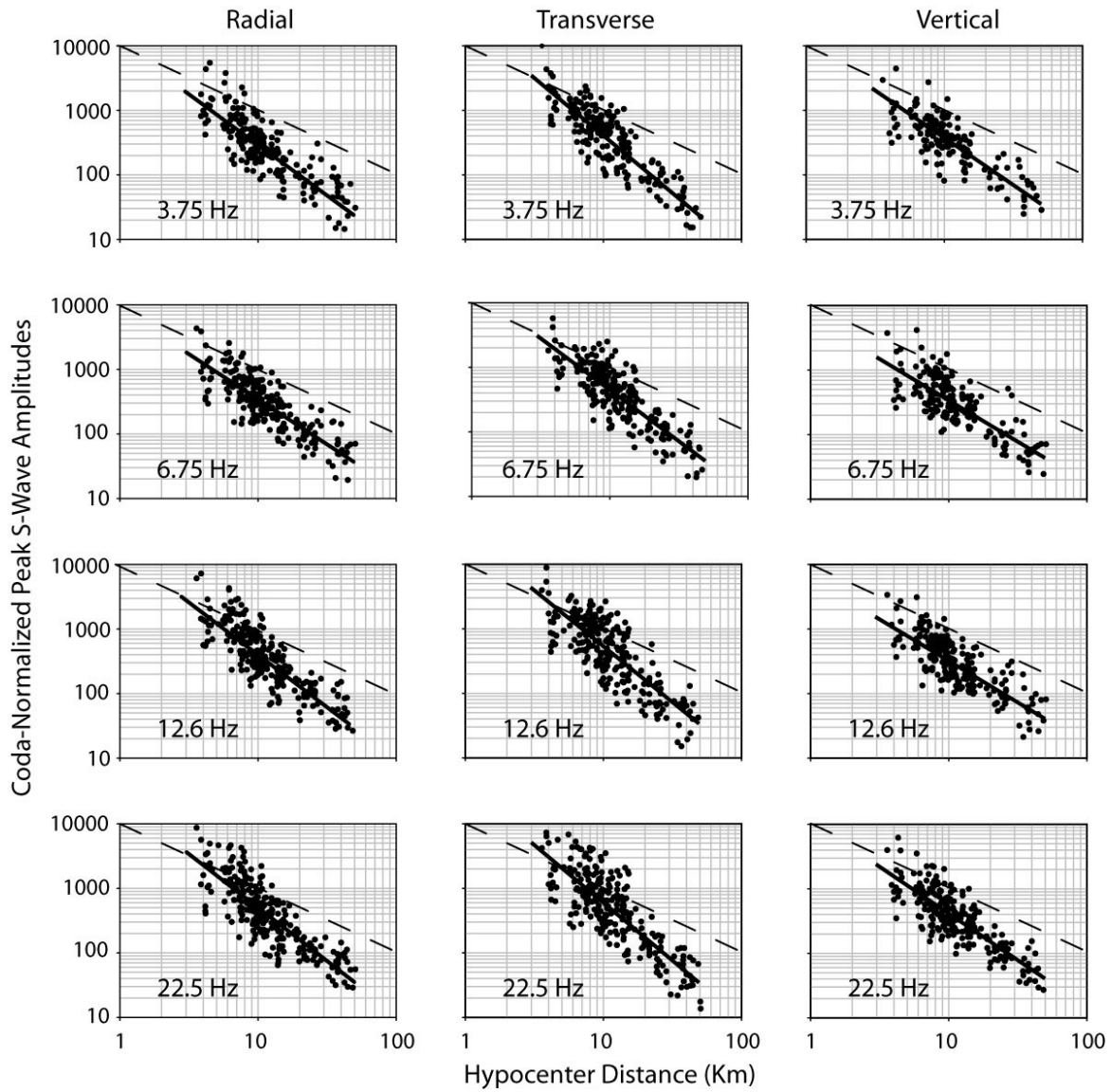


Figure 5. Plots of coda-normalized peak trace envelope amplitudes (filled circles) versus hypocenter distance in 4 octave-wide frequency bands, centered at 3.75, 6.75, 12.6 and 22.5 Hz. Left column shows radial component amplitudes, center column shows transverse component amplitudes, and the right column shows vertical component amplitudes. The solid lines show least-squares fits to the data. The dashed lines indicate the slope of expected log-amplitude versus log-hypocenter distance behavior for geometrical spreading in a homogeneous whole space.

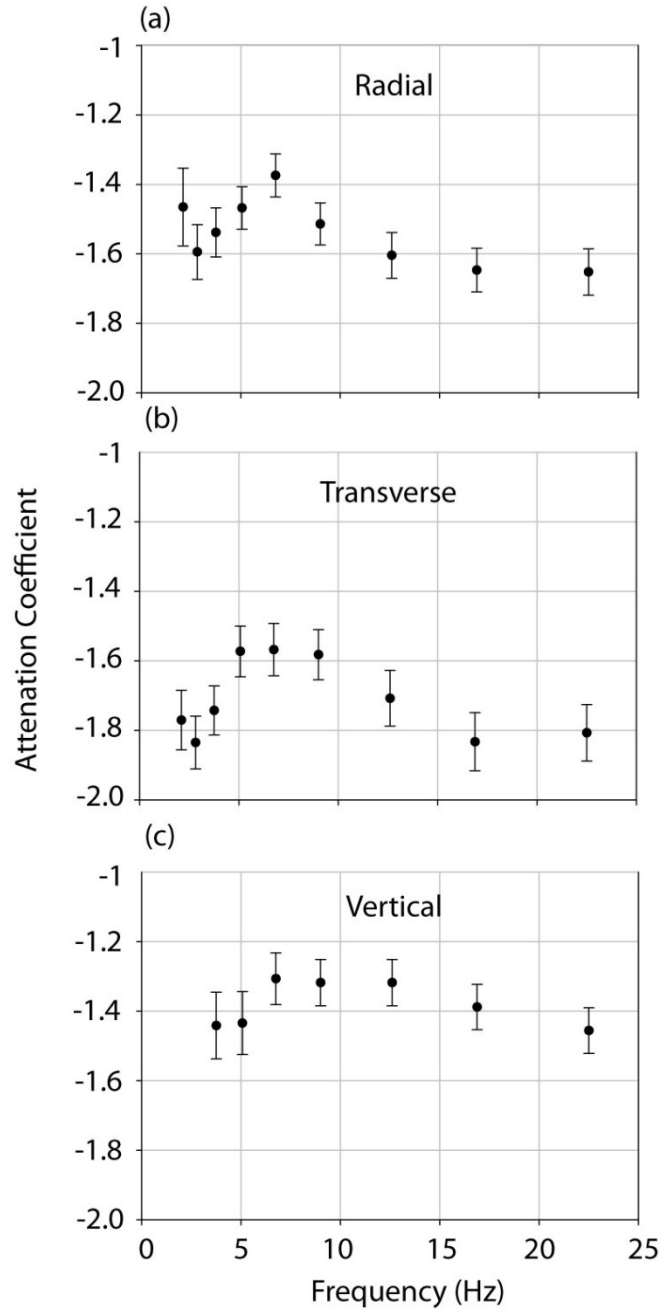


Figure 6: Estimates of the attenuation coefficient for peak S-wave ground motion in octave-wide frequency bands ($-\gamma$ in Equation 5) centered at 2.1, 2.8, 3.75, 5.1, 6.75, 9.0, 12.6, 16.9, and 22.5 Hz. Error bars indicate the \pm standard errors of estimate.

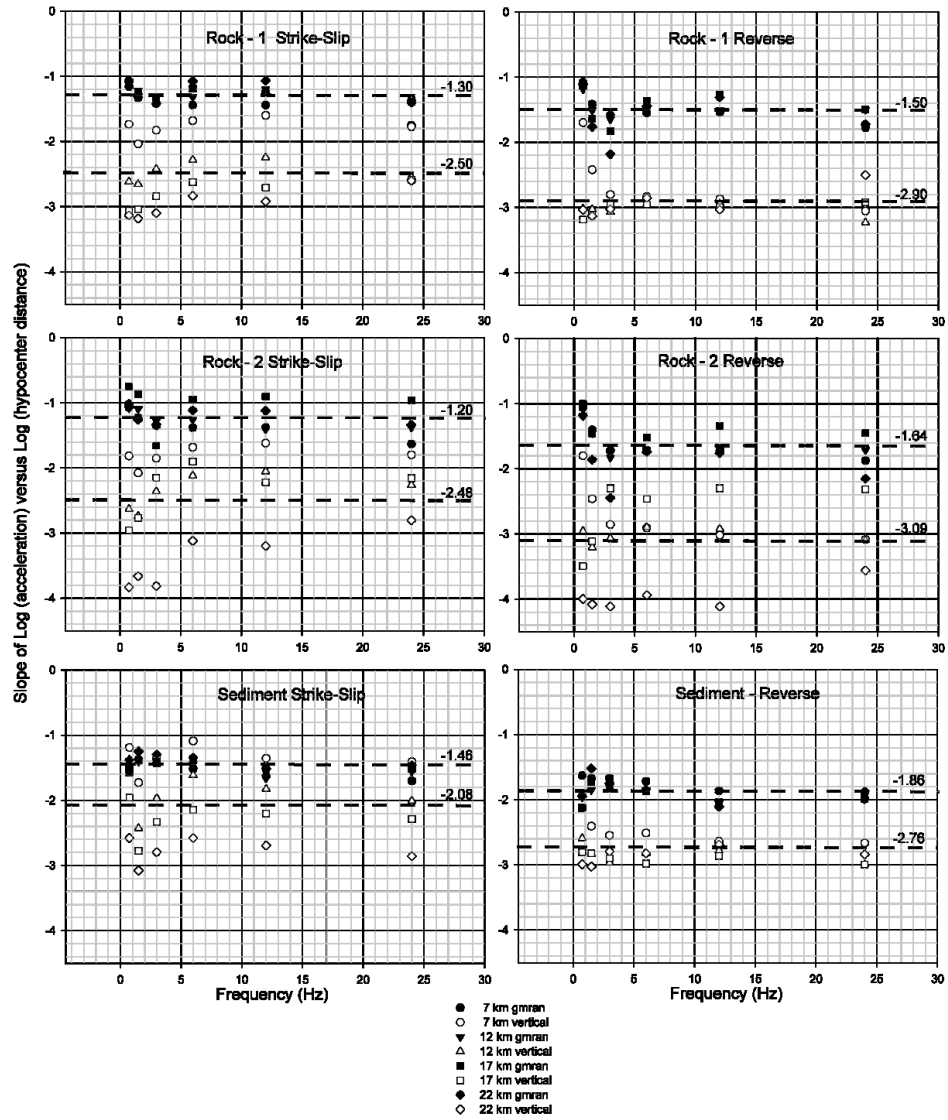


Figure 7. Results of theoretical modeling by Chapman and Godbee (2012). The slope of a linear regression of the logarithm of maximum acceleration on the logarithm of hypocenter distance for three velocity models, as a function of bandpass filter center frequency, for focal depths of 7.25, 12.25, 17.25 and 22.25 km, vertical and geometric mean of randomly oriented horizontal components. The values plotted are estimates of $-\gamma$ for attenuation as $r^{-\gamma}$, derived from full wavefield simulations in the hypocenter distance ranges 10-60 km, 18-60 km, 25-60 km and 33-60 km for focal depths 7.25 (circles), 12.25 (triangles), 17.25 (squares) and 22.25 km (diamonds), respectively. Filled symbols are for the geometric mean of the horizontal components, open symbols are for the vertical component. Dashed lines with numbers indicate mean estimates, averaged over focal depth and frequency. Adapted from Chapman and Godbee (2012).

Bibliography

- Aki, K. (1980). Attenuation of shear waves in the lithosphere for frequencies from 0.05 to 25 Hz, *Phys. Earth Planet. Int.*, 21, 50-60.
- Atkinson, G.M. (2004). Empirical attenuation of ground-motion spectral amplitudes in southeastern Canada and the northeastern United States, *Bull. Seism. Soc. Am.* **94**, 1079-1095.
- Atkinson, G.M. (1993). Notes on ground motion parameters for eastern North America: Duration and H/V ratio, *Bull. Seism. Soc. Am.*, 83, 587-596.
- Atkinson, G. and R. Mereu (1992). The shape of ground motion attenuation curves in southeastern Canada, *Bull. Seism. Soc. Am.* **82**, 2014-2031.
- Atkinson, G.M. and D.M. Boore (1995). New ground motion relations for eastern North America, *Bull. Seism. Soc. Am.*, 85, 17-30.
- Atkinson, G.M. and D.M. Boore (2006). Earthquake ground motion prediction equations for eastern North America, *Bull. Seism. Soc. Am.*, **96**, 2181-2205.
- Boore, D.M. (1983). Stochastic simulation of high-frequency ground motions based on seismological models of the radiated spectra, *Bull. Seism. Soc. Am.* **73**, 1865-1894.
- Boore, D.M. (2003). Prediction of ground motion using the stochastic method, *Pure Appl. Geophys.*, 160, 635-676.
- Chapman, M.C., (2013). On the Rupture Process of the 23 August 2011 Virginia Earthquake, *Bulletin of the Seismological Society of America*, 103, 613-628.
- Chapman, M.C. and R.W. Godbee (2012). Modeling Geometrical Spreading and the Relative Amplitudes of Vertical and Horizontal High-Frequency Ground Motions in Eastern North America, *Bulletin of the Seismological Society of America*, 102, 1957-1975.
- Davenport, K. K., J. A. Hole, D. A. Quiros, L. D. Brown, M. C. Chapman, L. Han, and W. D. Mooney (2015). Aftershock imaging using a dense seismometer array (AIDA) after the 2011 Mineral, Virginia earthquake, in *The 2011 Mineral, Virginia, Earthquake and its Significance for Seismic Hazards in Eastern North America*, Horton, J.W., Jr., Chapman, M.C., and Green, R.A., (Editors), Geological Society of America Special Paper 509, 273-284.
- Dreiling, Jennifer and W.D. Mooney (2015). Shear-wave velocity structure and attenuation derived from aftershock data of the 2011 Mineral, Virginia, earthquake, in *The 2011 Mineral, Virginia, Earthquake and its Significance for Seismic Hazards in Eastern North America*, Horton, J.W., Jr., Chapman, M.C., and Green, R.A., (Editors), Geological Society of America Special Paper 509, 81-94.
- Frankel, A. (2015). Decay of S-wave amplitudes with distance from earthquakes in the Charlevoix, Quebec area: Effects of radiation pattern and directivity, *Bull Seism. Soc. Am.*, Early Edition, vol. 105, no. 2a, doi 10.1785/0120140249, in press 2015.
- Frankel, A., A. McGarr, J. Bicknell, J. Mori, L. Seeber and E. Cranswick (1990). Attenuation of high-frequency shear waves in the crust: Measurements from New York state, South Africa, and southern California, *J. Geophys. Res.*, 95, 17,441-17,457.
- Hanks, T., and R.T. McGuire (1981). The character of high-frequency strong ground motion, *Bull. Seism. Soc. America*, 71, 2071-2095.
- Herrmann, R.B. and A. Kijko (1983). Modeling some empirical vertical component *Lg* relations, *Bull. Seism. Soc. Am.* **73**, 157-171.

- Kennett, B.L.N. (1986). *Lg* waves and structural boundaries, *Bull. Seism. Soc. Am.* **76**, 1133-1141.
- Siddiqi, J. and G.M. Atkinson (2002). Ground motion amplification at rock sites across Canada, as determined from the horizontal-to-vertical component ratio, *Bull. Seism. Soc. Am.*, **92**, 877-884.
- Toro, G.N., N. Abrahamson and J. Schneider (1997). Model of strong ground motion in eastern and central North America; best estimates and uncertainties, *Seism. Res Lett.* **68**, 41-57.
- Wang, C.Y. and R.B. Herrmann (1980). A numerical study of P-, SV-, and SH- wave generation in a plane layered medium, *Bull. Seism. Soc. Am.* **70**, 1015-1036.
- Wu, Qimin, and M.C. Chapman (2015). The Aftershock Sequence of the 2011 Mineral, Virginia, Earthquake: Temporal and Spatial Distribution, Focal Mechanisms, Regional Stress and the Role of Coulomb Stress Transfer, submitted to *Bull. Seism. Soc. Am.*